CW-EPR and ENDOR Study of Cytochrome c_6 from *Anabaena* PCC 7119

Inés García-Rubio,* Milagros Medina,† Richard Cammack,‡ Pablo J. Alonso,* and Jesús I. Martínez*
*Instituto de Ciencia de Materiales de Aragón, CSIC-Universidad de Zaragoza, Zaragoza, Spain; †Departamento de Bioquímica y Biología Molecular y Celular, Facultad de Ciencias, and Institute of Biocomputation and Physics of Complex Systems (BIFI), Universidad de Zaragoza, Zaragoza, Spain; and ‡Department of Biochemistry, King's College, University of London, London, United Kingdom

ABSTRACT The detailed analysis of the continuous-wave electron paramagnetic resonance and electron nuclear double resonance measurements on cytochrome c_6 from *Anabaena* PCC7119 reveals several electronic and structural properties of this hemeprotein. The oxidized protein shows two forms that differ in the arrangement of the residues that act as heme axial ligands. Information about the orientation of these residues is obtained for one of the forms, which turns out to differ from that found in the reduced protein from x-ray experiments. The biological significance of these results is discussed.

INTRODUCTION

Physical techniques have been widely used in the study of the structure-function relationship of proteins. Among them, EPR and EPR-related techniques have provided a very useful tool for the analysis of metalloproteins involved in redox processes (see, for instance, Lowe (1) and Hoffman (2)). These techniques give information about the electronic structure of the metals present in proteins, as well as about their close environment, both of which are usually relevant for protein function. Additionally, ENDOR and ESEEM allow us to resolve hyperfine structures not seen in conventional CW-EPR, thereby improving the knowledge of the paramagnetic center structure.

Hemeproteins have been characterized by EPR since the first stages of its development, nearly 50 years ago (3). Among them, cytochromes of type *c* constitute an important group due to the critical biological functions they have as electron carriers involved in many vital processes, including photosynthesis, cell respiration, detoxification, and apoptosis (4). Cytochromes *c* usually display a CW-EPR signal in the oxidized (Fe^{3+}) state corresponding to the low spin $S = 1/2$ iron configuration, with a very anisotropic (rhombic) Zeeman interaction. A large number of cytochrome *c* CW-EPR spectra can be found in the literature; however, in many cases, they were reported only to determine the corresponding *g* principal values or to support the axial coordination of the heme (5–10). The lack of any resolved hyperfine interaction in the CW-EPR spectrum precludes more detailed information about the electronic structure of the heme center. Alternatively, EPR-related techniques such as ENDOR or ESEEM may reveal weak hyperfine interactions with adjacent (^1H, ^{14}N) nuclei. Nevertheless, relatively few works using these methods to study cytochromes or related heme systems have been reported (11–17).

Cytochromes c_6 are low-molecular-mass, monomeric, low-spin, soluble cytochromes *c*, which function as electron carriers between the cytochrome b_6f complex and the P700 reaction center of Photosystem I in cyanobacteria and green algae (18). In the case of the cyanobacterium *Anabaena* PCC 7119, plastocyanin acts as the preferred electron carrier in this reaction, but it is replaced in this function by cytochrome c_6 when a shortage of copper in the medium prevents synthesis of enough plastocyanin (18). Cytochromes c_6 from several species, including *Anabaena* PCC 7119, have been characterized by means of several techniques, including CW-EPR, NMR, and x-ray diffraction (7,10,19–24), providing information about the heme structure in different states. Unusual CW-EPR spectra have been reported for some of them, such as pH dependence of the EPR signal or coexistence of different EPR forms. EPR spectra of *Anabaena* cytochrome c_6 have been reported at pH values ranging between 5 and 11 (19). These spectra were analyzed on the basis of the Taylor model (25), and estimations of the crystal field parameters Δ/λ and V/λ were obtained (19). The study also raised some open questions:

1. Two EPR forms coexist, and they are dependent on the pH (19,20). Similar behavior has been described in several cytochromes (5,7). In the case of cytochrome c_6 from *Anabaena*, the coexistence of two different protein forms has been detected in NMR measurements, indicating that the EPR observations are not just a consequence of the frozen state (20). However, only one pH-dependent reduction potential has been described for the protein (19).
2. At pH 7, the spectra allowed the principal *g*-tensor values ($g_X = 1.43$, $g_Y = 2.29$, $g_Z = 2.94$) for one of the two

Submitted December 23, 2005, and accepted for publication June 5, 2006.

Address reprint requests to Jesús I. Martínez, Facultad de Ciencias, Universidad de Zaragoza, C/ Pedro Cerbuna 12, E-50009 Zaragoza, Spain. Tel.: 34-976-762460; Fax: 34-976-761229; E-mail: jimartin@unizar.es.

Inés García-Rubio's present address is Laboratory of Physical Chemistry, ETH Hönggerberg, CH-8093 Zürich, Switzerland.

Abbreviations used: EPR, electron paramagnetic resonance; ENDOR, electron nuclear double resonance; ESEEM, electron spin echo envelope modulation spectroscopy; CW, continuous wave; NMR, nuclear magnetic resonance; ei, echo induced; LS, low-spin; HALS, highly anisotropic low-spin.

0006-3495/06/09/2250/14 $2.00

doi: 10.1529/biophysj.105.080358

coexisting forms to be directly obtained, but only the low-field feature ($g_3 = 3.3$) of the other form could be unambiguously assigned. A very broad feature at $g_{ef} = 2.05$ was tentatively assigned to the intermediate principal g-factor (g_2) and the third one was estimated ($g_1 = 1.05$) using the empirical formula $g_X^2+g_Y^2+g_Z^2 = 16$ (26).

3. The heme axial coordination was analyzed in terms of the crystal field parameters Δ/λ (tetragonal field) and V/Δ (rhombicity). This technique was introduced (27,28) as a semiempirical method to predict the likely ligands to low-spin heme. For *Anabaena* cytochrome c_6, the crystal field parameters corresponded to a bis-histidine axial coordination. In fact, on the basis of sequence and structure comparisons, the iron in *Anabaena* cytochrome c_6 actually displays methionine-histidine axial coordination.

The nature and mechanistic relevance of these observations has not yet been established. As the coexistence of different forms of cytochrome c_6 in vivo could have important functional consequences, a supplementary effort in CW-EPR characterization is necessary to resolve these open questions.

ENDOR spectroscopy may also help to provide a better understanding of the electronic structure of the heme center within the protein environment. This technique allows the measurement of weak hyperfine coupling to the paramagnetic species. Some ENDOR studies for characterizing hemeproteins, iron-porphyrin model complexes, and other heme systems have been reported (11,12,14–16,29). In such studies, interactions of the electronic spin with some of the nitrogen and hydrogen nuclei surrounding the iron atom have been reported. Additionally, if a reliable three-dimensional environment of the studied heme group is known, the point dipole interaction term can be calculated. These calculations are considered a good approximation for the actual dipolar coupling with nuclei distant by >0.25 nm (30) and have been used, in combination with the contact hyperfine interaction part as estimated from NMR studies, to compare the evaluated proton frequencies with experimental ENDOR results in some heme systems (12). These data provide valuable information about the electronic structure of the heme environment, in particular by estimating the g-tensor principal directions.

In this article, we present a study of cytochrome c_6 from *Anabaena* PCC 7119 using EPR spectroscopy and ^{1}H-ENDOR. We will focus on samples at pH <7.5, as the acidic region is more relevant from a mechanistic point of view.

MATERIALS AND METHODS

Protein purification and EPR sample preparation

Cytochrome c_6 was purified from the cyanobacterium *Anabaena* PCC 7119, as previously described (19,31). After purification, a mixture of oxidized and reduced species is obtained, since cytochrome c_6 from *Anabaena* does not spontaneously oxidize in the presence of O_2. We have also observed that several conditions induce the autoreduction of a proportion of the molecules and that the two reduction states show distinct behavior in a CM-Cellulose column. Similar observations have been made in cytochromes c_6 from other species (32). Therefore, complete oxidation of the sample before EPR measurements was required. Samples obtained after purification were fully oxidized by adding an excess of ferricyanide. After oxidation ferri- and ferrocyanide were removed from the sample by successively concentrating and replacing the buffer using Centricom tubes (Amersham, Piscataway, NJ). The final oxidized concentrated sample was prepared in HEPES buffer, 50 mM, pH 7, which was used as solvent in the experiments described. When indicated, glycerol was also added to the solvent (up to 30% by volume). Samples were transferred into quartz EPR tubes of 3-mm internal diameter. Dissolved molecular oxygen, which might produce a spurious broad EPR signal, was removed by flushing the EPR tubes under an argon flow system for 30 min. Samples were immediately frozen and stored at 77 K.

EPR and ENDOR measurements

CW-EPR and ei-EPR spectra were recorded on a Bruker (Karlsruhe, Germany) ESP380 spectrometer working at X-band. An Oxford (Eynsham, UK) CF935 continuous-flow cryostat was used. Typical measurement conditions for CW-EPR were temperature, 15 K; modulation amplitude, 0.4 mT; and microwave power, 0.1 mW. For ei-EPR, the standard two-pulse and three-pulse sequences were used, and the spectrum was recorded with fixed τ and t values and collecting the echo intensity while the magnetic field is swept.

ENDOR measurements were recorded on a Bruker ESP300 spectrometer with a Bruker ENDOR accessory with a 500 W radiofrequency amplifier and frequency modulation, and an Oxford ESR900 continuous flow cryostat. Typical measurement conditions were temperature, 6 K; and microwave power, 5 mW.

Calculation of hyperfine constants using the point dipole approximation

Hyperfine interaction parameters can be straightforwardly calculated if both electron and nuclear spins are considered as point magnetic dipoles (30). In such a situation, the hyperfine Hamiltonian can be divided into

$$H = H_{iso} + H_{dip},$$

where the H_{iso} ''contact'' term is

$$H_{iso} = A_{iso}\,\vec{S}\,\vec{I},$$

where A_{iso} is the isotropic hyperfine constant, and $\vec{S}$ and $\vec{I}$ the electronic and nuclear spins (in the case of ^{1}H coupling to low-spin heme, $S = 1/2$ and $I = 1/2$).

The anisotropic H_{dip} part is described by

$$H_{dip} = \frac{\vec{\mu}_e\,\vec{\mu}_n}{r^3} - \frac{3(\vec{\mu}_e\,\vec{r})\,(\vec{\mu}_n\,\vec{r})}{r^5},$$

where $\vec{r}$ is the vector connecting the iron atom with the interacting proton. The associated electronic ($\vec{\mu}_e$) and nuclear magnetic ($\vec{\mu}_n$) moments are defined as

$$\vec{\mu}_e = -\mu_B\,\tilde{g}\,\vec{S},$$
$$\vec{\mu}_n = \mu_N\,g_N\,\vec{I},$$

where μ_B, μ_N, g_N, and $\tilde{g}$ are the Bohr magneton, the nuclear magneton, the proton g-factor, and the electronic g-tensor, respectively.

In particular, simpler expressions can be derived for hyperfine splitting when the proton hyperfine interaction is weak in comparison with Larmor

frequency ν_L, and the magnetic field points toward one of the $\tilde{g}$ principal directions. In this case, two ENDOR signals associated with each interacting proton are detected, at frequenciesν_+ and ν_-:

$$\nu_{\pm} = \nu_L \pm \frac{A_{ii}}{2},$$

where i stands for one of the principal directions X, Y, or Z. The hyperfine splitting is then obtained as

$$A_{ii} = A_{iso} + (A_{dip})_{ii},$$

where $(A_{dip})_{ii}$ is

$$(A_{dip})_{ii} = \frac{\mu_N \mu_B g_N g_i}{r^3}(3\cos^2\theta - 1),$$

and θ is the angle between the magnetic field vector, $\vec{B}$, and $\vec{r}$.

Preliminary x-ray diffraction studies of the three-dimensional structure of *Anabaena* (ferro)cytochrome c_6 (P. Legrand, unpublished data) supply values of distance and orientation of each proton relative to the iron center ($\vec{r}$ vector) for our calculations. These x-ray studies reveal just one structure for the heme environment. Coordinates of the atoms in the heme group and in the iron axial ligands His-18 and Met-58, as well as some relevant distances and angles, are displayed as Supplementary Material. Fig. 1 *A* shows the notation used for the nitrogen and carbon atoms in heme, His, and Met moieties, and Fig. 1 *B* depicts the heme environment. Since protons are not detected in the x-ray structure, their positions were calculated from the appropriate bonding direction assuming a C (or N)-H distance of 0.11 nm.

Computer simulation of ENDOR spectra

To confirm the analysis of the experimental ENDOR signals, computer simulations of the spectra at different magnetic field positions were done. The software package used for EPR spectroscopy was EasySpin, version 2.5.0. This is free software developed by the EPR group of the Eidgenössische Technische Hochschule Zürich (33).

General conditions for simulations were excitation line width, 200 MHz; and g-strain, 10%. For other conditions specific for each proton, see Table 6 and text.

EXPERIMENTAL RESULTS AND ANALYSIS

EPR spectra

Fig. 2 *A* shows the CW-EPR spectrum of *Anabaena* cytochrome c_6 at 15 K, similar to that previously reported (19). The spectrum shows the characteristic features of form I and form III (34); we hereafter label these as LS and HALS, respectively. The features corresponding to the principal g-factors of the LS form ($g_X = 1.45$, $g_Y = 2.31$, $g_Z = 2.94$) and the only recognizable feature for the HALS form ($g = 3.30$) are indicated. Additionally, a narrow signal at $g_{ef} = 2.05$ is also seen in the spectra (see Fig. 2 *A*). It is found that the intensity of this signal relative to the other in the spectrum changes from one sample to another.

We have made additional effort to fully characterize the HALS form. To reduce the inhomogeneous signal-broadening related to ice crystal formation, ''g-strain'' (35), which has been shown to affect aqueous samples of cytochromes, the spectrum was also recorded in the presence of glycerol as a vitrifying agent. EPR spectra of cytochrome c_6 in the presence of glycerol showed small shifts of the features as well as a narrowing of all the signals except the one at $g_{ef} = 2.05$ (Fig. 2 *B*). The latter effect is particularly shown by the $g_{ef} = 3.30$ signal from the HALS form, which displays a relative increase in height in comparison with the $g_{ef} = 2.96$ peak from the LS form. Additionally, a broad feature at $g_{ef} = 1.91$ was also clearly distinguished.

The effects of temperature and microwave power changes on the spectral features of these EPR spectra were also analyzed. Increasing the temperature caused a broadening of

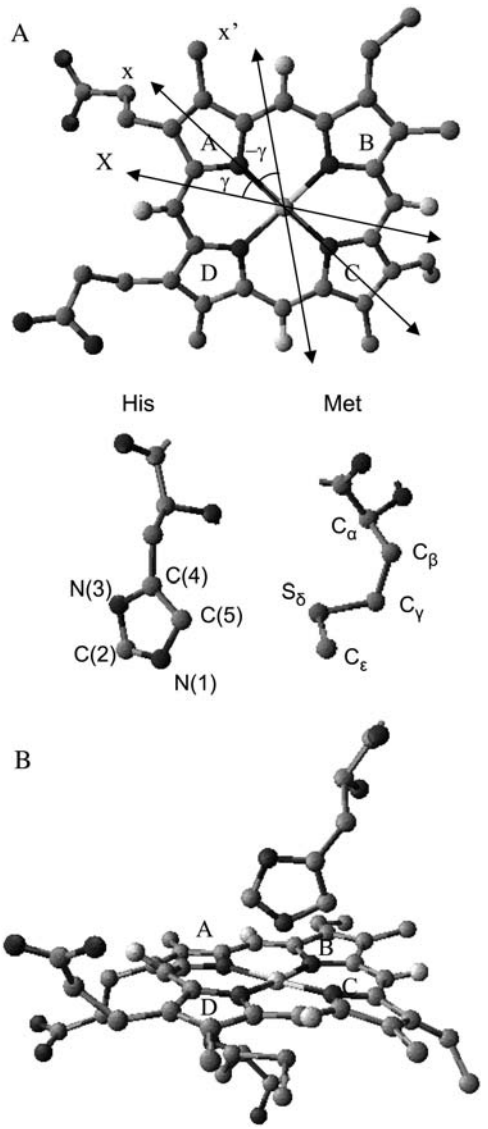

FIGURE 1 Three-dimensional model of the heme group in *Anabaena* cytochrome c_6. (*A*) Scheme of the heme plane and axial residues, with the nomenclature for the heme nitrogens and residue carbons and nitrogens, and a draft of the three used axis frames. The x (molecular), x' (electronic), and X (magnetic) axes are indicated with the rotation/counterrotation angle $\gamma/-\gamma$. The $z \equiv z' \equiv Z$ axis is perpendicular to the plane, and the y, y', and Y axes are in the plane, perpendicular to x, x', and X, respectively. (*B*) Three-dimensional model showing the heme group as observed in the x-ray diffraction model of the heme *Anabaena* PCC 7119 (ferro)cytochrome c_6.

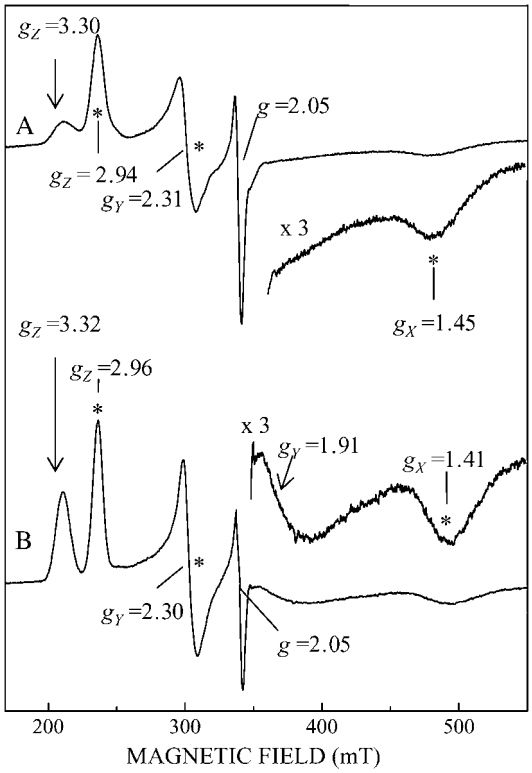

FIGURE 2 X-band EPR spectra of oxidized cytochrome c_6 from *Anabaena* PCC 7119 at 15 K: (*A*) HEPES buffer, 50 mM, pH 7; (*B*) HEPES buffer, 50 mM, pH 7, with 30% glycerol. Asterisks mark the three features corresponding to the principal g-factors of the LS form, and arrows features corresponding to the principal g-factors of the HALS form (see text). g_{ef} factors are shown for each relevant signal. High-field region of the spectra is magnified to show g_Y and g_X features.

the signals. This effect is more pronounced for $g_Z = 3.30$ and $g_{ef} = 1.91$ features and they became unobservable at temperatures >50 K (spectra not shown). The three features due to the LS form ($g_X = 1.45$, $g_Y = 2.31$, and $g_Z = 2.94$) were observed up to 80 K, whereas at higher temperatures only the $g_{ef} = 2.05$ signal could be detected. Increasing microwave power induced a partial saturation of the LS features (and of the $g_{ef} = 2.05$ signal as well), whereas the $g_{ef} = 1.91$ and $g_{ef} = 3.30$ signals showed a linear dependence throughout the accessible power range. These results strongly suggest that the $g_{ef} = 1.91$ signal corresponds to the intermediate principal g-factor of the HALS form. All the evidence points to the $g_{ef} = 2.05$ signal as being due to a paramagnetic impurity. As has been indicated, it shows no correlation with the behavior of other spectral features. Even its relative intensity varies from one sample to another when they come from different purifications. Other authors also detected the same signal in other cytochrome *c* samples, and they assigned it to an exogenous (probably copper) center (7,8).

The high-field feature (g_X) of the HALS form still remains undetectable in the CW-EPR spectrum. To overcome this limitation, ei-EPR experiments on *Anabaena* cytochrome c_6 at 6 K were carried out (Fig. 3). The ei-EPR technique produces an apparent ''absorption mode'' CW-EPR spectrum by measuring the electron echo during a magnetic field sweep (30), sometimes allowing detection of broad unresolved signals in CW-EPR spectra. The ei-EPR spectra of *Anabaena* cytochrome c_6 allows a straightforward identification of the three features of the LS form, the low-field g_Z feature of the HALS form, and the spurious signal at $g_{ef} = 2.05$. In the sample containing glycerol, the g_Y feature of the HALS form ($g_Y = 1.91$) is also revealed (Fig. 3). Moreover, the echo signal is still observed in the low-g-value magnetic-field region. Depending on the specific τ (2p), or τ- and t-values (3p), ei-EPR spectra sometimes show apparent ''features'' as the one in 650 mT for 2p in Fig. 3. These are due to echo modulations, and change from one spectrum to another. However, the echo signal is still detected at magnetic field values >1200 mT. This echo must be due to the HALS species. Above the shoulder feature in the ei-EPR spectra (high-field arrow in Fig. 3), echo intensity decays to zero for all τ- and t-values.

Thus, ei-EPR allows detection of the high-field part of the HALS signal that is not seen in conventional CW-EPR spectra. Therefore, the complete set of principal g-tensor parameters for the two coexisting *Anabaena* cytochrome

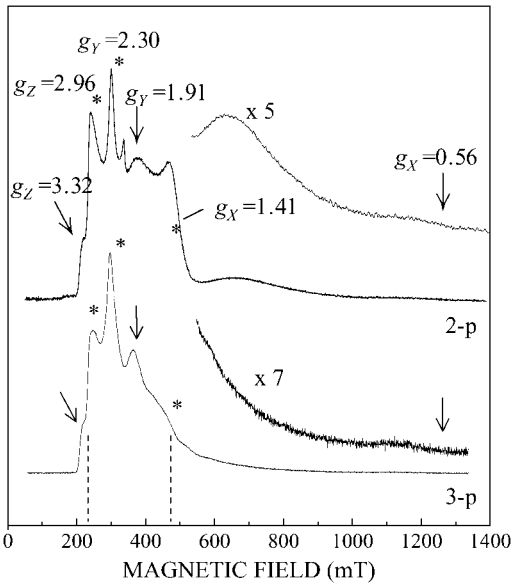

FIGURE 3 Two-pulse (τ = 96 ns) (*upper*) and three-pulse (τ = 96 ns, t_1 = 208 ns) (*lower*) ei-EPR spectra of *Anabaena* PCC 7119 cytochrome c_6 at 6 K in 50 mM HEPES, pH 7, and 30% glycerol. The LS form features are marked with stars and the features assigned to the HALS form with arrows. The high-field regions are magnified. The small peak between $g_{ef} = 2.30$ and $g_{ef} = 1.91$ corresponds to a paramagnetic impurity, and the broad feature at 650 mT in the two-pulse spectrum is caused by echo modulation and does not correspond to a CW-EPR feature, as is demonstrated by the persistence of the echo up to 1.3 T (see text). It must be noted that in the field region between the two dashed lines there is EPR absorption from the two cytochrome forms.

c_6 forms, at pH 7, LS and HALS, is obtained (Table 1). The values given here are slightly shifted with respect to those previously reported, owing to the decrease of the ''g-strain'' effect. It must be pointed out that the empirical formula $g_X^2+g_Y^2+g_Z^2 = 16$ is not fulfilled by the HALS form g-tensor principal values here determined for *Anabaena* cytochrome c_6. This formula has usually been applied to systems where one of the principal values cannot be obtained directly from experiments, but it does not have theoretical support from the heme electronic ground state description, as the equations in Taylor's study (25) show that the quantity $g_X^2+g_Y^2+g_Z^2$ can reach any value between 12 and 16. Some known heme systems give a value close to 16, but there are several exceptions reported in the literature (33,36).

It has been suggested that the coexistence of the two EPR forms might be produced by ''in vitro'' oligomerization. To clarify this point, and following Campos et al. (7), a study was carried out concerning the dependence of the intensity of the EPR signals on protein concentration. Fig. 4 shows that no change in the relative intensity of HALS and LS forms is observed upon increasing protein concentration. If oligomerization had taken place, the relative intensity of the oligomer signal upon decreasing protein concentration by 100 times might be expected to be reduced to $<10\%$, depending on the dissociation constant. The effect of ionic strength on the putative oligomerization was also analyzed by determining the relative intensities of the LS and HALS forms as a function of the ionic strength of the medium (between 0 and 300 mM of NaCl in the sample buffer), but no major changes were detected (not shown). These results suggest that in the case of *Anabaena* cytochrome c_6, the coexistence of HALS and LS forms is not related to protein oligomerization.

Another interesting question relates to the quantification of the abundance of each EPR form. Previous studies on *Anabaena* cytochrome c_6 considered the HALS form to be minor in comparison with the LS form (19). In other cases (7,37), estimation of the relative abundance of cytochrome c_6 forms from their superimposed EPR signals has been performed using the methods outlined in DeVries and Albracht (26) and Aasa and Vänngård (38). Such methods are good for obtaining quantitative information about the total spectral intensity from the area under the g_Z absorption-like peak when the spectra fulfill several conditions about the linewidth and aspect of the signals. However, in our case, the area under these peaks cannot be determined with accuracy because they are partially superimposed, and the g_Z peaks are not narrow enough. Therefore, the measured spectrum would allow at best a semiquantitative estimate of the relative abundance of the EPR forms. An estimate of the relative abundance of the two forms in several samples of *Anabaena* cytochrome c_6 from their EPR spectrum, using the method described by Aasa and Vänngård (38), yielded values from 30% to 70% abundance for the HALS form, depending on the way of determining the reference baseline and the actual areas of the g_Z peaks. In samples with glycerol for the HALS form, a value near the higher end of this range was usually obtained. Although imprecise, this study demonstrated that none of these signals is ''residual'', and that the HALS form might even be the predominant form.

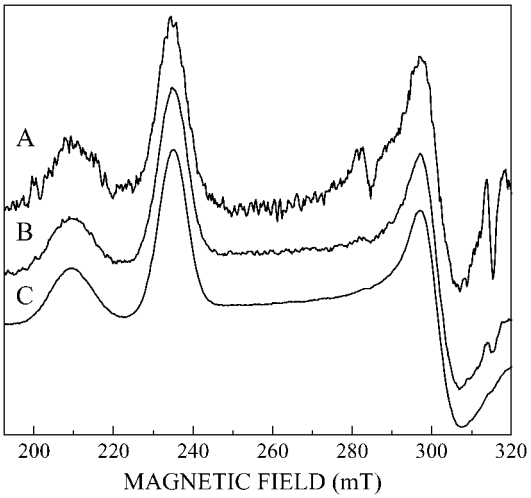

FIGURE 4 Detail of the X-band EPR spectra of *Anabaena* PCC 7119 cytochrome c_6 at different protein concentrations: (*A*) 50 μM; (*B*) 500 μM; (*C*) 5 mM. Some (cavity) spurious signals are seen in spectra *A* and *B* due to the very low protein concentration.

TABLE 1 *g*-factors, state coefficients, and distortion parameters for the two (ferri)cytochrome c_6 EPR forms of *Anabaena* PCC 7119

Form	g_X*	g_Y*	g_Z*	$a^\dagger$	$b^\dagger$	$c^\dagger$	$\Delta/\lambda^\S$	$V/\Delta^\S$
LS	1.41	2.30	2.96	0.95	0.28	0.16	2.7	0.64
HALS	0.56	1.91	3.32	0.86	0.45	0.22	2.2	0.37

*The sign of the g-factor is not experimentally determined; absolute values are given.

†The set of coefficients a, b, and c is chosen among those compatible with the g-factors for giving a normalized ground electron wave function (see Taylor (25)).

§Distortion parameters correspond to proper axes (see text).

Since all the principal values of the effective g-tensor of both coexisting forms of *Anabaena* cytochrome c_6 have been obtained (Table 1), the distortion parameters, Δ/λ and V/λ, of the Griffith model (3,25) can be estimated (Table 1). As already shown for some cytochromes, parameters for the LS form disagree with the actual His-Met axial coordination and the region in the crystal field diagram (27) that their distortion parameters are expected to occupy (7,8,10). Certainly, the crystal field diagram is not theoretically rigorous but is a semiempirical approach. For the reported cases of cytochromes similar to the LS form, a question about the distortion axis choice has to be considered. Δ/λ and V/λ parameters depend on the choice of the distinguished axis for the main ''axial'' distortion. The original version of the crystal field diagram formalism used improper axes (that is, axes for which the additional rhombic distortion was larger

than that of the main axis). It might be more logical to adopt a proper axis election, for which $0 \leq |V/\Delta| \leq 2/3$ (33,39). For all the known heme systems, selecting the axis perpendicular to the heme plane (namely the z axis) as the main distortion axis leads to a proper distortion frame. We have reconstructed the crystal field diagram based on those arguments, and separate regions for the different axial coordinations again appear (Fig. 5). Most of the conclusions obtained by Blumberg and Peisach (27) from the crystal field diagram are valid with this new version, but the position that the LS form occupies in the diagram is now between His-Met and His-His regions; this indicates that these two regions do not show a distinct boundary, but tend to overlap.

When the orientation of the principal axes of the g-tensors (hereafter magnetic axes X, Y, and Z) is known, the principal values of the effective g-tensor provide information about the electronic distribution in the ground state Kramers doublet. A particularly simple picture is reached in the case, verified for all the cytochrome heme centers described, where the Z magnetic axis lies nearly normal to the heme plane ($Z \equiv z$), whereas the other two (X and Y magnetic axes) lie in the heme plane and make an angle γ with the N-Fe bonding directions (which define the x and y molecular axes, see Fig. 1 *A*). In this case, a basis set of the ground state that determines the $|+\rangle$ and $|-\rangle$ states of the $S_{ef} = ½$ spin is given by

$$|+\rangle = ad_{x'z}\alpha - ibd_{y'z}\alpha - cd_{xy}\beta$$
$$|-\rangle = ad_{x'z}\beta + ibd_{y'z}\beta + cd_{xy}\alpha,$$

where the (x', y', z') frame is defined from the molecular x, y, and z axes by a $-\gamma$ rotation around the normal to the heme plane (see Fig. 1). The spinors α and β are referred to as the (x', y', z'), and $d_{x'z}$, $d_{y'z}$, and d_{xy} have the usual meaning. It is worth noting that although the orbital d_{xy} is the standard form of a t_{2g} d-orbital referred to as the molecular axes, $d_{x'z}$ and $d_{y'z}$ are obtained by a rotation around the z molecular axis from the standard d_{xz} and d_{yz} orbitals. The coefficients a, b, and c that define the ground state Kramers doublet are related to the principal g-tensor values by expressions similar to those derived by Taylor (25) (for a detailed description of the derivation of g-values as a function of a, b, and c coefficients; see García-Rubio et al. (17), Supplementary Material, and references therein). In Table 1, we have also collected the values of such coefficients estimated for both EPR forms of cytochrome c_6. It can be seen that the ground state of the LS form displays a very high $d_{x'z}$ character, whereas the HALS form shows an admixture, especially of the $d_{y'z}$.

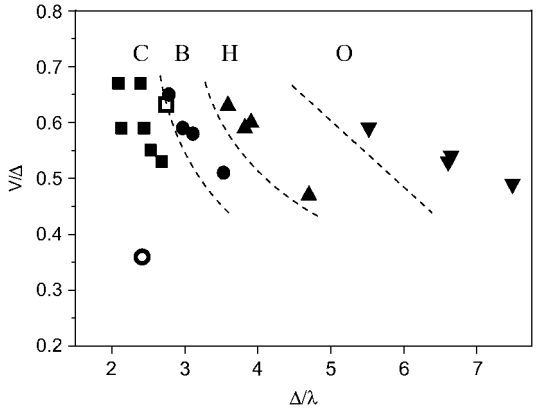

FIGURE 5 ''Crystal field diagram'' for distortion parameters in proper axes. Some of the points in the original diagrams of Blumberg and Peisach (27) have been recalculated in proper axes to determine the new regions. The region names used in Blumberg and Peisach (27), which correspond to specific axial coordination of the heme, have been used: (*C*) His-Met; (*B*) His-His; (*H*) His-imine N; (*O*) His-OH^-. Distortion parameters for LS (*open square*) and HALS (*open circle*) forms of *Anabaena* PCC 7119 cytochrome c_6 are also represented.

ENDOR experimental results

ENDOR spectra of *Anabaena* cytochrome c_6 were recorded at magnetic field values corresponding to the g-tensor principal values of the HALS and LS EPR signals. The microwave absorption region of the LS form overlaps with the region of absorption of the HALS signal (Fig. 3). This implies that when measuring ENDOR spectra at field positions in the LS resonance range, ENDOR signals from both EPR forms are expected. Measurements at field values <225 (below the magnetic field corresponding to the LS g_Z value), or >460 mT (above the LS g_X value), display only HALS ENDOR features. However, this is expected to be a small contribution, since, as can be observed in Fig. 3, the relative amplitude of the LS form in the superposition region is always significantly higher (approximately four times more intense in the ei-EPR spectrum, except for the HALS g_Y position, where we do not report the ENDOR spectrum). Therefore, it can be assumed that the LS paramagnetic centers make the major contribution to the ENDOR spectra obtained in this field range. Such an assumption is supported by two experimental facts: 1), no ENDOR signal has been detected at magnetic fields higher than the LS g_X (which would be associated with the HALS form); and 2), our measurements have been adequately interpreted by using just one set of hyperfine interactions that correspond to a single heme center. On the other hand, the ENDOR signal detected at 205 mT ($g_{ef.} = 3.3$) must correspond to the HALS species, because there is no detectable EPR LS signal intensity at this field (the linewidth of the LS g_Z feature is ~8 mT).

Hereafter, for the sake of brevity, the ENDOR spectra will be labeled by the g principal value corresponding to the selected field position. To distinguish the signals coming from exchangeable protons, each spectrum was recorded in samples containing either H_2O or D_2O (substitution of ~95%) as solvent.

Fig. 6 shows the g_Z ^1H ENDOR spectra of the LS and the HALS forms of cytochrome c_6. All the spectra are

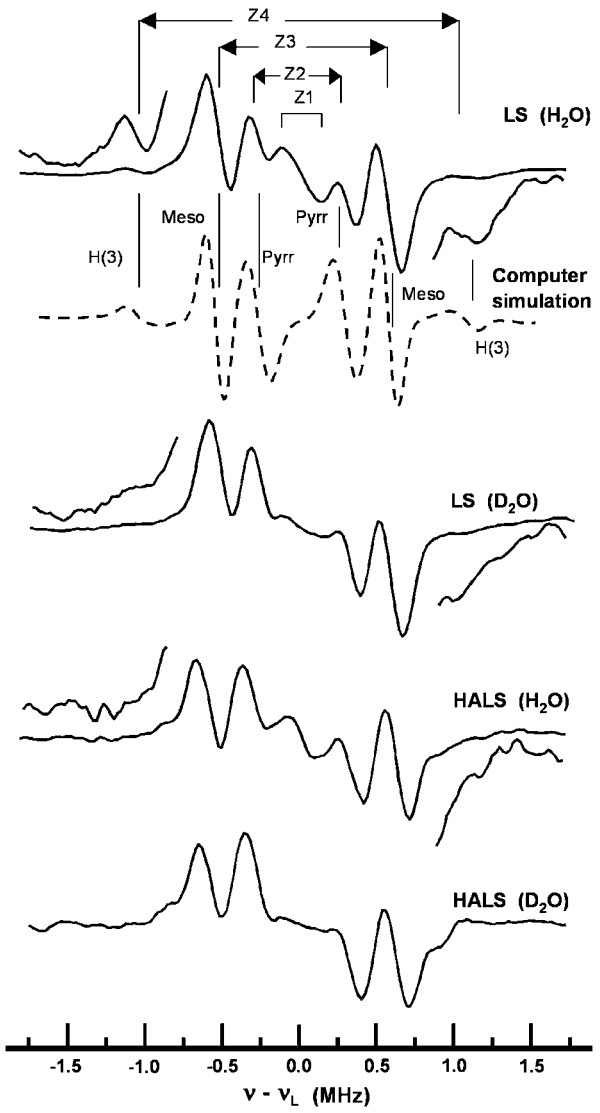

FIGURE 6 X-band ENDOR spectra at g_Z field for LS and HALS forms of cytochrome c_6 from *Anabaena* PCC7119. Splittings discussed in the text are labeled as indicated in Table 1. The regions corresponding to the Z4 splitting in spectra of LS (H_2O), LS (D_2O), and HALS (H_2O) have been magnified. It can be seen that Z4 is due to an exchangeable proton and that it is not present in the HALS form. Computer simulation of the LS form with water as solvent is also displayed in the dashed trace. Simulation parameters are shown in Table 6 and Materials and Methods. The proton interaction that contributes mainly to each signal in the simulated spectrum is specified (for details, see text).

symmetrically distributed around the ^{1}H Larmor frequency (ν_L), indicating that the effective ^{1}H hyperfine constant, A_{ZZ}, is $<2\nu_L$. In such a case, the distance between related peaks directly provides the value of A_{ZZ} (Tables 2 and 3) (see Materials and Methods). Comparison of spectra in H_2O and D_2O indicates that the signals with A_{ZZ} ~0.3 MHz (numbered Z1) in both LS and HALS forms are due to exchangeable protons. These weakly interacting exchangeable proton signals are observed in all ENDOR spectra when H_2O is used as solvent and are considered to come from remote protons of the solvent. The other proton signals that remain in D_2O spectra are assigned to nonexchangeable protons. Significantly, the g_Z LS ENDOR spectrum presents a stronger interacting exchangeable proton, signal Z4, $|A_{ZZ}| = 2.32$ MHz, not detected in the HALS spectrum. Otherwise, most of the observed splittings are almost identical in the ENDOR spectra of the LS and HALS forms.

TABLE 2 Experimental parameters for the LS EPR form from ENDOR measurements at the g_Z field position

$\|A_{ZZ}\|_{exp}$ (MHz)	Figure label	Assignment	$(A_{dip})_{calc}$ (MHz)*	A_{iso} (MHz)†
0.28 ± 0.10	Z1	Remote H	–	–
0.62 ± 0.05	Z2	Methyl H in pyrrole	−0.67	0.05
1.18 ± 0.05	Z3	Meso H	−1.30	0.12
2.32 ± 0.05	Z4	H(3)?	–	–

*Values for A_{dip} have been calculated using the distances and orientations from the heme environment in the x-ray structural model of *Anabaena* PCC 7119 (ferro)cytochrome c_6 (P. Legrand, unpublished data).
†A_{iso} is the difference between $(A_{ZZ})_{exp}$, with the appropriate sign (12), and A_{dip} (see Materials and Methods).

The g_Y and g_X ^{1}H ENDOR spectra were only recorded for the LS form (Figs. 7 and 8, respectively), since no ENDOR signal could be detected in the field corresponding to g_X of HALS and, moreover, the signals found in the field value corresponding to g_Y were attributed to the LS form (see above). Comparison of spectra in H_2O and D_2O indicates that the only exchangeable signals are those derived from remote protons with $A_{eff} \approx 0.3$ MHz. As in the g_Z ENDOR spectra, the signals are symmetrically disposed around the ^{1}H Larmor frequency and the effective hyperfine coupling constants (Tables 4 and 5) can be directly derived from the spectra.

Assignment of ENDOR spectra signals

Proton ENDOR coupling was analyzed by calculation of the hyperfine couplings as described in Materials and Methods using the heme environment structural data of the (ferro)cytochrome c_6 (see Supplementary Material and Fig. 1). The structure of the reduced protein might be different from the

TABLE 3 Experimental parameters for the HALS EPR form from ENDOR measurements at the g_Z field position

$(\|A_{ZZ}\|)_{exp}$ (MHz)	Assignment	$(A_{dip})_{calc}$ (MHz)*	A_{iso} (MHz)†
0.23 ± 0.10	Remote H	–	–
0.67 ± 0.05	Methyl H in pyrrole	−0.76	0.09
1.30 ± 0.05	Meso H	−1.48	0.18

*Values for A_{dip} have been calculated by using the distances and orientations from the heme environment in the x-ray structural model of *Anabaena* PCC 7119 (ferro)cytochrome c_6 (P. Legrand, unpublished data).
†A_{iso} is the difference between $(A_{ZZ})_{exp}$, with the appropriate sign (12), and A_{dip} (see Materials and Methods).

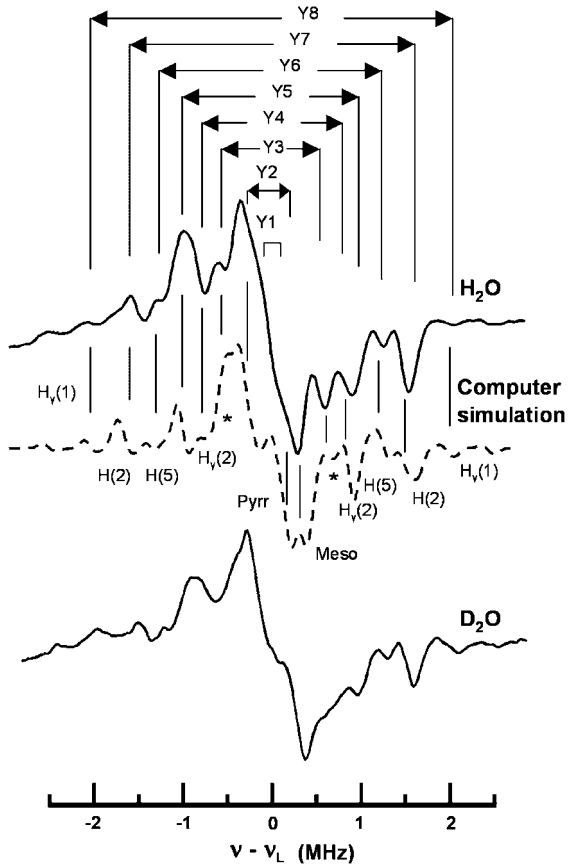

FIGURE 7 X-band ENDOR spectra at g_Y field for LS form of cytochrome c_6 from *Anabaena* PCC 7119. Splittings discussed in the text are labeled as indicated in Table 4. Computer simulation of the LS form with water as solvent is also displayed in the dashed trace. Simulation parameters are shown in Table 6 and Materials and Methods. The proton interaction that contributes mainly to each signal in the simulated spectrum is specified (for details, see text). Asterisks mark relatively weak signals in the simulated spectrum, where several proton interactions are contributing.

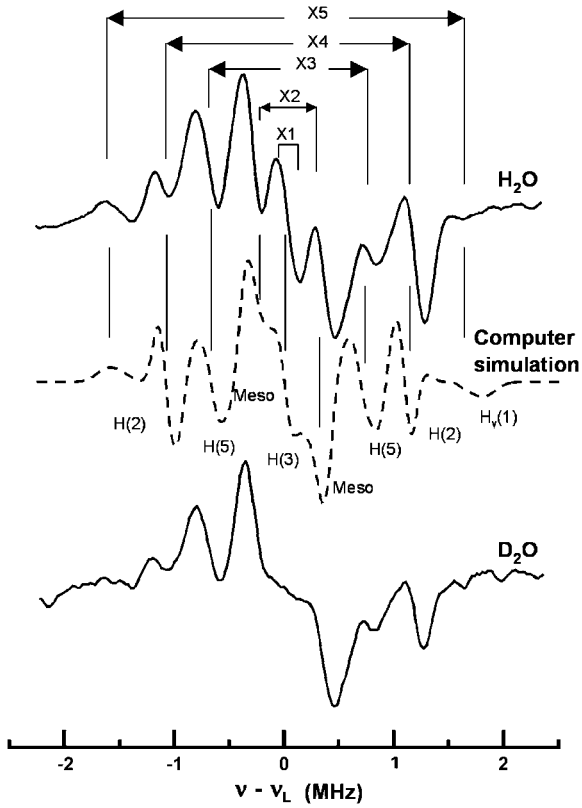

FIGURE 8 X-band ENDOR spectra at g_X field for LS form from cytochrome c_6 of *Anabaena* PCC 7119. Splittings discussed in the text are labeled as indicated in Table 5. Computer simulation of the LS form with water as solvent is also displayed in the dashed trace. Simulation parameters are shown in Table 6 and Materials and Methods. The proton interaction that contributes mainly to each signal in the simulated spectrum is specified (for details, see text).

oxidized state of the ENDOR measurements. The crystallographic electron density map was fitted to just one structure and one heme environment, whereas we detected two forms (LS and HALS) coexisting in the oxidized state. However, due to its rather rigid structure, we can consider that the iron-proton positions in the porphyrin ring are invariant. Our ENDOR experiments can give some insight into the relationship of LS and HALS heme environments with that of the reduced protein structure. Besides, information about the orientation of the g tensor principal axes can be extracted.

As a first step, the contact contribution to the hyperfine coupling of the nearby protons was determined from the g_Z ENDOR spectra, where the magnetic field is perpendicular to the heme plane. In Scholes et al. (12), it is shown that the nonexchangeable ^{1}H signal observed in the g_Z ^{1}H ENDOR spectra are due to ''weakly interacting'' protons of the methyl substituents of the pyrroles and mesoprotons, both in the porphyrin ring. For these protons, the angle θ between the Fe-H direction and the magnetic field is $\sim$90° and from their distances to the iron the dipolar interaction $(A_{dip})_{calc}$ is readily calculated (see Materials and Methods). The contact contribution A_{iso} is obtained by subtracting the dipolar contribution from the experimental values of A_{ZZ}. The calculated dipolar contribution and the subsequently estimated contact contributions derived are given in Tables 2 and 3.

The Z4, $|A_{ZZ}| = 2.32$ MHz, signal (exchangeable proton) in the LS g_Z spectrum should also be assigned. The three-dimensional structure of the reduced *Anabaena* cytochrome c_6 heme environment shows that His-18 and Met-58 coordinate the iron in its axial positions (Fig. 1 *B*). This preliminary model suggests that in the neighborhood of the paramagnetic species only the hydrogen atom bound to N(3) of His-18, hereafter H(3), is exchangeable. The H(3) point-dipole contribution to the hyperfine interaction calculated from the structure is 1.8 MHz, smaller than the experimental one. This might indicate that the heme environment shown by the x-ray structure (in the reduced state) differs from the oxidized LS structure. Another possibility might be that the H(3) contact interactions were notably different from that reported by Scholes et al. (12), showing indeed a change in

TABLE 4 Experimental parameters for the LS EPR form from ENDOR measurements at the g_Y field position

$\lvert A_{exp}\rvert$ (MHz)	Figure label	Assignment
0.4 ± 0.1	Y1	Remote H
0.6 ± 0.1	Y2	Meso/pirrole
1.0 ± 0.1	Y3	Meso?
1.5 ± 0.1	Y4	Meso/Met H
1.9 ± 0.1	Y5	Met H
2.5 ± 0.1	Y6	His H(5) ⊥
3.2 ± 0.1	Y7	His H(2) ⊥
4.2 ± 0.1	Y8	Met H_γ ⊥

its sign. This would imply a drastic modification of the electronic density distribution of the LS form of cytochrome c_6 in comparison with other cytochromes and model heme complexes. Alternatively, the splitting of 2.32 MHz might be due to a water molecule close to the heme center in the LS oxidized form. The HALS form does not display the large $|A_{ZZ}| \approx 2.3$ MHz, suggesting a structural difference between the LS and HALS forms.

In the ENDOR spectrum at the g_Y position, all the signals detected, except for the one showing the smallest splitting, are due to nonexchangeable protons. Their effective hyperfine coupling constant values are collected in Table 4. To assign these signals, it is important to keep in mind that it is not a single crystal-like spectrum, as is the case for g_Z and g_X ENDOR spectra. All of the centers with an orientation fulfilling the following equation contribute to the g_Y ENDOR spectra:

$$g_{ef}^2 = (g_X^2\cos^2\varphi + g_Y^2\sin^2\varphi)\sin^2\theta + g_Z^2\cos^2\theta,$$

where θ and φ represent, respectively, the colatitude and azimuth angle of the magnetic field direction referred to as the g-tensor principal axes. Since there is not a single orientation to calculate the point dipole hyperfine contribution, assignment of the g_Y ENDOR signals is a difficult task. Besides, at this field position the expressions for calculating hyperfine interaction from point dipole approximation in the case of weak interaction and g principal direction (see Materials and Methods) are no longer valid; they can just be seen as a rough approach. Nevertheless, in a multiorientational ENDOR spectrum, and especially in those close to the g_Y field position, perpendicular features (that is, features with an angle between the magnetic field and the proton-iron direction $\theta = 90°$, see Materials and Methods) of axial hyperfine interactions are often detected (12). They are usually identified, as they display a nearly constant signal position when ENDOR spectra are measured at different field positions around g_Y, whereas signals corresponding to nonperpendicular features shift or disappear when the field is varied. Keeping this in mind, several ENDOR spectra for g_{ef} positions between g_Y (2.30) and 2.60 were recorded (not shown). In all these spectra, the features labeled, in Table 4 and Fig. 7, Y2–Y8 were preserved, indicating that they may correspond to perpendicular features. Thus, we can proceed with the assignment of these signals. As the value for θ for the perpendicular features is determined to be 90°, point dipole calculations of A_{dip} depend just on the proton-iron distance. The splitting detected at 4.2 MHz (signal Y8) was not observed in the model complex spectra shown in Scholes et al. (12). The calculations show that it corresponds to an interacting proton at a distance of ~0.28 nm to the iron, assuming a negligible contact hyperfine term. This distance is compatible with one of the protons in the γ position of the Met-58 residue in the reduced cytochrome c_6 structure (see Supplementary Material), which would also explain why the signal does not appear in bis-His model complex measurements (12). Signals with a splitting of 3.2 MHz and 2.5 MHz (Y7 and Y6) should correspond to perpendicular features of H(2) and H(5) protons, respectively, of the His residue, as they are similar to the splittings seen in some heme systems and assigned in Scholes et al. (12). The similarity of these perpendicular splittings would indicate that the distances of H(2) and H(5) to the iron (0.32 nm), as well as the contact term, are similar. The distances derived from the structure in the reduced protein are 0.31 and 0.32 nm, respectively. Differences observed in distances can be attributed to the fact that the imidazole ring is slightly tilted with respect to the normal of the porphyrin plane in the cytochrome c_6 three-dimensional model. The other peaks observed in the ENDOR spectra can be assigned to protons in the porphyrin ring or in Met-58. Distances to the iron of mesoprotons and pyrrole methyl substituent protons, together with the isotropic part determined from the g_Z spectra, are compatible with couplings of 0.6 MHz and 1.0 MHz (signal Y2 and Y3), respectively. The other two pairs of spectral lines, Y4 and Y5, which show splittings of 1.6 MHz and 1.9 MHz, can be assigned to protons at distances between 0.36 and 0.40 nm. Several proton nuclei in the Met-58 residue should be located at similar distances.

TABLE 5 Experimental parameters for the LS form from ENDOR measurements at the g_X field position

$(\lvert A_{XX}\rvert)_{exp}$ (MHz)	Figure label	Assignment
0.3 ± 0.1	X1	Meso/pirrole/remote
0.7 ± 0.1	X2	Meso H
1.6 ± 0.1	X3	His H(5)
2.5 ± 0.1	X4	His H(2)
3.2 ± 0.1	X5	Met H_γ

With regard to the ^{1}H ENDOR spectra at g_X of LS (Fig. 7), we consider that all the signals detected correspond to the LS form. As pointed out above, all the signals except X1 are associated with nonexchangeable hydrogen nuclei. The effective hyperfine coupling constant of the ^{1}H ENDOR signal are summarized in Table 5. As with g_Z, the g_X spectrum corresponds to a single orientation; therefore, only molecules whose g_X axis is oriented along the magnetic field contribute to the ENDOR spectrum. As we have seen for g_Z, in the case of a single crystal-like spectrum the calculation of the point dipole contribution to the hyperfine interaction is

straightforward, and again we can use this as a basis for assigning the ENDOR signals to the protons in the neighborhood of iron. However, unlike the g_Z, the g_X principal axis is in principle an unknown direction in the heme plane. As it usually differs from one low-spin heme center to another, the splittings can be very different and consequently the assignment of the lines cannot be made based on the ones found in the literature. This fact makes it more difficult to get computed values for the interactions to compare with experimental results, but when the assignment is feasible, it provides valuable structural information of the heme center environment. Since we have already estimated from the g_Z spectrum the contact contribution of the hyperfine interaction for the porphyrin protons (see Table 2), the expected A_{XX} hyperfine parameters can be calculated just by computing the dipolar part and adding them. On this basis, we have calculated the expected A_{XX} hyperfine parameters for the porphyrin protons as a function of the g_X principal axis orientation on the porphyrin plane. It is worth remembering that the proton positions are determined by the porphyrin ring structure, and the calculation depends just on one angle γ that determines the g_X direction in the plane (Fig. 1 *A*). The results of such calculations are plotted in Fig. 9. Protons located at opposite positions with respect to the iron atom are expected to have the same interaction and their ENDOR lines will coincide for any field orientation. So, for any field direction, two pairs of lines with different hyperfine splitting will arise from the four mesoprotons, whereas three pairs of lines will come from the four methyl substituents of the heme *c* pyrroles. From Fig. 9 two conclusions can be readily obtained: First, signals >1.6 MHz, X3–X5, do not come from porphyrin ring protons, as they are too large; and second, the splitting of signal X2, 0.7 MHz (*shadow stripe*) is compatible with mesoproton coupling. In Scholes et al. (12), a small coupling signal (in their case, ~1 MHz) in the g_X ENDOR spectra of one model complex is also detected. Although the authors do not comment on it, all the other signals in their spectrum were assigned to coupling of protons of axial ligands, so this one is implicitly considered to come from porphyrin protons.

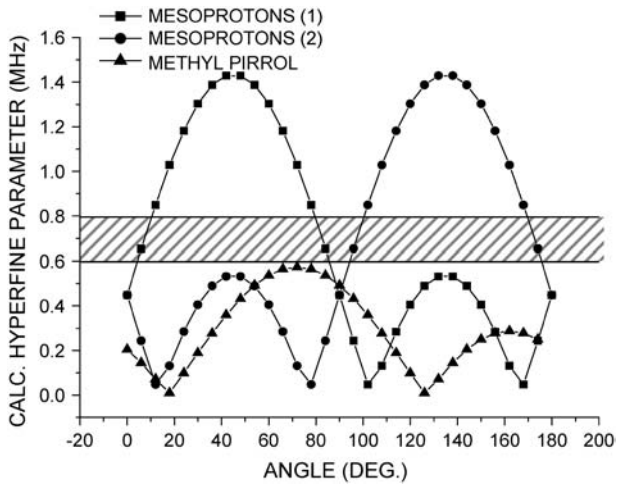

FIGURE 9 Calculated hyperfine splitting (calculated dipolar contribution plus experimental isotropic part derived from g_Z results) of the two couples of equivalent mesoprotons and one of the methyl substituent of the pyrrole, as a function of the in-plane g_X axis orientation (determined by the clockwise angle from the NA-NC direction). The horizontal shadow stripe shows the experimental weak coupling splitting from g_X ENDOR (see text).

Fig. 9 indicates that our calculations lead to an estimation of the g_X direction in the porphyrin plane (superposition of calculated coupling of mesoprotons and measured 0.7 MHz splitting). It would form a small γ angle (~8°) with one of the N-Fe-N bonding directions. In a previous study, it was estimated from NMR measurements that the rhombic distortion axis in *Anabaena* cytochrome c_6 makes an angle of 10° with the NA-Fe-NC direction (20). Since the rhombic distortion direction (Fig. 1 *A*) is related to the g_Y principal direction by counterrotation with respect to the N-Fe-N direction, the g_X principal direction is expected to be close to the NB-Fe-ND direction (17,40), which would be fully consistent with our results.

Now we can assign the larger experimental g_X splittings. Features in the g_X ENDOR spectra of model complexes that correspond to H(2) and H(5) couplings have been previously detected (12). The coupling of the two protons detected in our g_Y measurements are similar to that obtained by Scholes et al. (12), and provide values for the contact hyperfine terms ($A_{iso} = -0.9$ MHz for H(2) and $A_{iso} = -0.3$ MHz for H(5)) and distances to the iron (both 0.32 nm). However, the angle between their iron-proton direction and g_X is not known. H(2) and H(5) are expected to be symmetrical with respect to the N(His)-Fe bonding (which is nearly perpendicular to the porphyrin ring), but the orientation of the imidazole ring projection on the porphyrin plane varies from one heme system to another and can be different from the one obtained for the reduced cytochrome structure. We estimated the hyperfine coupling (sum of the contact and dipolar part) for the two protons H(2) and H(5) as a function of the angle that the imidazole projection on the prophyrin plane makes with the g_X axis. The result is depicted in Fig. 10. The experimental values for signals X3 and X4, 1.6 MHz and 2.5 MHz, respectively, are marked as stripes. Fig. 10 shows that H(2) and H(5) splittings are restricted below 2.5 MHz. It is most likely that splittings of 1.6 MHz and 2.5 MHz obtained from the g_X spectrum correspond to those His-18 protons, as there seem to be no other protons in the structure to account for those splittings, in particular for the one at 2.5 MHz. Fig. 10 shows that an orientation of the His imidazole ring plane forming an angle of ~75–80° is compatible with the ENDOR results. This conclusion has to be considered with care in view of the assumptions made about the imidazole ring position for the calculations, but it provides an estimate of the ring orientation. On the other hand, the position of His-18 in the structural model of the heme environment of (ferro)cytochrome c_6 (Fig. 1 *B* and Supplementary

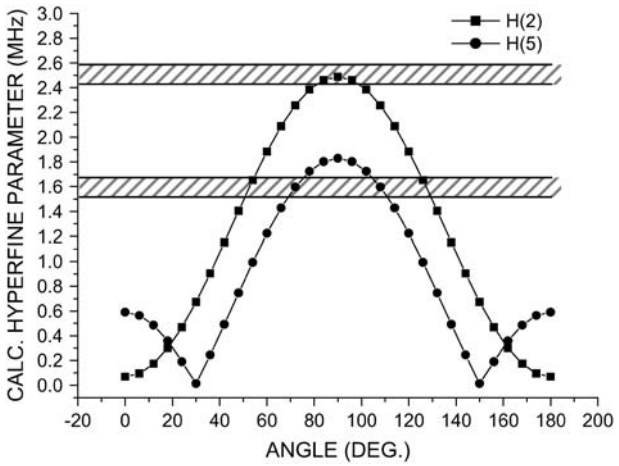

FIGURE 10 Calculated hyperfine splitting, calculated using the dipolar contribution plus the isotropic part derived from g_Y results and Scholes et al. (12), of the protons bound to C(2) and C(5) of the His-18 imidazole ring, as a function of the angle between the g_X axis orientation and the imidazole plane projection on the porphyrin plane. The imidazole plane was supposed to be perpendicular to the porphyrin plane and symmetric with respect to the N(1)-Fe axis (see text). The horizontal shadow stripes show the two experimental splittings (2.5 MHz and 1.6 MHz) from g_X ENDOR (see text).

Information) would predict splittings for both H(2) and H(5) protons of 0.4 MHz, a value that is incompatible with the experimental one. This analysis suggests that there are different conformations for this His residue between the oxidized and reduced *Anabaena* cytochrome c_6.

Let us focus now on the highest detected splitting, signal X5, 3.2 MHz, in the g_X ENDOR spectrum. Examination of the structure of the heme environment in cytochrome c_6 indicates that the closest proton to the iron at 2.7–2.8 Å should be one at position γ in the Met residue, and therefore a likely candidate for the largest splitting observed in the g_X spectrum. The dipolar contribution to its hyperfine interaction, calculated from the structural data for the reduced protein is just $(A_{dip})_{XX} \approx 2.8$ MHz, but such a value could be drastically increased by a modest rearrangement of the Met residue consistent with a small change in the orientation and preserving the H_γ-Fe distance. It should be noted that in these calculations the actual distance is in the limit of validity of the point dipole approximation, and we do not know the corresponding ''contact'' part. However, this is consistent with the previously described results for the H_γ proton of Met in the g_Y ENDOR spectrum.

To confirm the previously described ENDOR analysis, we calculated computer simulations of the experiments. Simulated ENDOR spectra for the three g principal directions can be seen in Figs. 6–8. It must be remembered that the CW-ENDOR experiment depends on the electronic and nuclear relaxation times in a complex way that is not implemented in standard simulation software. A fair fitting between simulation and experiment can usually be obtained for the signal positions, but the actual widths and intensities are only approximated.

A set of seven groups of interacting protons has been used in simulations: mesoprotons (four protons divided in two groups of two protons related by a 90° rotation in the porphyrin plane); methyl protons in pyrrole (four sets of three protons related by rotations in the porphyrin plane as seen in Fig.1); protons bound to C(2), N(3), and C(5), H(2), H(3) and H(5), respectively, of His-18; and the two protons bound to C_γ of Met-58 (the closest protons to iron in this residue). The parameters used are collected in Table 6. Parameters for mesoprotons, pyrrole protons, H(2) and H(5) are fully derived from our previous analysis. H(3) was

TABLE 6 Parameters for the computer simulations of the ENDOR spectra

g_X axis:	
$\varphi = 98°$	
Mesoprotons:	Pyrrole methyl substituent protons:
$r = 4.4$ Å	$r = 5.8$ Å
$\theta = 90°$	$\theta = 90°$
$A_{iso} = 0.12$ MHz	$A_{iso} = -0.03$ MHz
lw (g_Z) $= 0.20$ MHz	$lw = 0.20$ MHz
lw (g_Y) $= 0.25$ MHz	
lw (g_X) $= 0.15$ MHz	
H(2) His proton:	H(5) His proton:
$r = 3.18$ Å	$r = 3.20$ Å
$\theta = 48°$	$\theta = 48°$
$\varphi' = 77°$	$\varphi' = 68°$
$A_{iso} = -0.80$ MHz	$A_{iso} = -0.05$ MHz
$lw = 0.15$ MHz	$lw = 0.15$ MHz
H(3) His proton:	H_γ(1) Met proton:*
$r = 4.9$ Å	$r = 2.7$ Å†
$\theta = 15°$	$\theta = 133°$†
$\varphi' = 85°$	$\varphi' = 4°$†
$A_{iso} = 0.5$ MHz	$A_{iso} = 1.4$ MHz
$lw = 0.20$ MHz	$lw = 0.15$ MHz
H_γ(2) Met proton:*	
$r = 3.5$ Å†	
$\theta = 148°$†	
$\varphi' = 47°$†	
$A_{iso} = 0.2$ MHz	
$lw = 0.15$ MHz	

The positions of the protons relative to the Fe atom and isotropic hyperfine parameter have been fixed for the spectra calculated in all the field positions, except that linewidths have been modified in some cases. Positions and isotropic hyperfine parameters can show slight changes with respect to the values obtained in the analysis (always within the error bar), as a result of the refinement process. The following symbols and abbreviations are used: r, distance from Fe to H; θ, angle between the Fe-H direction and the Fe-N(His) direction; for protons in the porphyrin ring, the orientation for g_X and g_Y ENDOR spectra are determined from the angle between the g_X axis and N(A)-Fe-N(C) direction, φ; for His and Met protons, the angle between the projection of the Fe-H direction into the porphyrin plane and the g_X axis, φ', is also specified; lw, ENDOR signal linewidth.

*Protons bound to C_γ of the Met residue. They are the closest to the Fe atom.

†Data obtained directly from x-ray structure of reduced cytochrome c_6 of *Anabaena* PCC7119.

included to demonstrate that its interaction could explain the Z4 signal. However, the A_{iso} parameter for this proton should be very different from that obtained by other authors; thus, we think that the possibility of explaining this signal with a solvent proton or others cannot be discarded. For Met protons, positions in the reduced cytochrome form were used. Small changes in the structure could cause a drastic variation of the dipolar part of their hyperfine interaction; thus, the A_{iso} parameters used cannot be considered true from our evidence, but again the simulations show that these protons could account for the measured signals.

Each contribution to the simulated spectrum was calculated separately, and the final simulation is obtained simply by adding all of them. The contributions are added without any additional factor for correcting relative intensities, except for pyrrole contributions, which need to be multiplied by a factor of ~0.1–0.3 to reproduce the experimental intensities. This is probably because relaxation times involved in their ENDOR transitions are quite different (maybe due to the methyl dynamics) from those for the other protons.

Many of the signals in simulated spectra (especially for the g_Y position) are due to the superposition of lines due to several interactions. In the figures, the main contribution has been used to label them. Besides the good general agreement between experiments and calculations, we want to emphasize two points: H(2), H(5), and Met proton contributions to the g_Z spectrum are so weak that they cannot be resolved, as had been previously predicted (12), and the possible contribution of H(3) to the g_Y and g_X spectra would be always in the very small splitting region.

The good agreement of the simulated spectra with the experimental ones confirms our analysis, and specifically the g frame and His orientations obtained from the experimental evidence.

DISCUSSION

The results collected in the previous section can be discussed in relation to the structure of reduced cytochrome c_6, and in particular with that of the heme center in the different redox states. First we will explore the structural meaning of the difference between the two oxidized forms, LS and HALS. From the experimental g-factors, distortion parameters for both forms were obtained (Table 1). It can be seen that the HALS form shows a small shift for the Δ/λ parameter and a larger decrease of V/Δ with respect to the parameters of the LS form (Fig. 5). Moreover, the evidence indicates that the LS and HALS EPR forms both correspond to heme centers with a His-Met coordination. It is well established that axial ligands of the heme are mainly responsible for the distortion parameters. The effect of ligand asymmetry on the rhombic field can be increased because some ligand orientations induced a distortion in the planar porphyrin ring (34). Several studies on model complexes and proteins have determined the origin of the LS and HALS forms in bis(imidazole) and bis(pyridine) heme centers (36,41,42). It was found that bis-His systems with high rhombicity (similar to our LS form) display the two imidazole planes nearly parallel, and a planar porphyrin ring. On the other hand, in HALS forms imidazole planes are almost mutually perpendicular and the porphyrin ring is ruffled. The HALS configuration displays a drastic reduction of the rhombic distortion parameters, and a small reduction of the axial parameter, consistent with our findings. The effect of Met and His axial residues on the rhombic parameter has also been discussed for other cytochromes c and model compounds by several authors (6,43). The nature and strength of the influence of the Met residue on the distortion parameters remains controversial, but it is clear that the differences between the two LS and HALS forms that we detect in cytochrome c_6 of *Anabaena* have to come from differences in the conformation of the axial ligands, most probably because of their orientation with regard to the heme plane.

The coexistence of two EPR forms implies that there are two conformations of the protein in the sample. The two forms are present in comparable abundance. In other cytochromes c, there are many examples of pH-dependent interconversion of two or more EPR forms (5,7,10). These processes usually show pK_a values >7, and are associated with proton exchanges in the heme vicinity, or even to ligand replacement. It is worth noting that those pH-dependent interconversions often allow the coexistence of both forms in a broad range of pH values, and in particular at the physiological pH. In one case, it was described that the addition of a detergent to the sample eliminated one of the coexistent forms (7). Cytochrome c_6 from *Anabaena* PCC7119 shows a more complex behavior. The coexistence of the LS and the HALS forms is not pH-dependent, but both forms show another pH-dependent interconversion into forms termed III to III′ and I to II, in the nomenclature of Medina et al. (19), with the same pK_a values. This indicates that a similar process (possibly the exchange of a specific proton) takes place in both forms at the same pH value. The coexistence makes it difficult to characterize each form separately. The protein showed only one redox potential (19), and so far, the preliminary x-ray data reveal only one reduced heme environment. NMR studies on this protein were also not easy to interpret. At low pH values, NMR spectra were described as due to a single form. At higher pH values, the behavior in oxidized samples was more complex and not completely understood (19,20). In NMR spectra, reduced samples showed no modification with pH. The behavior is similar to that observed in cytochrome c_6 from *Monoraphidium braunii*, where the two EPR forms coexist in a pH-dependent equilibrium with essentially equal reduction potentials. An explanation for the experimental evidence is that the two forms are in a dynamical equilibrium in solution. The rate of interconversion might not be observed in NMR studies in solution, but would affect the EPR and ENDOR measurements in frozen samples.

Our ENDOR results provide further insight into the structure of the heme in the oxidized LS form. As described above, we have obtained the g tensor principal axes for this form, which are related to the distortion directions. The values obtained are compatible with the distortion axes obtained from previous NMR studies (20). On the other hand, we have demonstrated that the orientation of the axial ligand in the LS form, in particular the His residue, is different from that proposed in the structural model of the reduced heme environment. Our results suggest that g_X and g_Y are close to the in-plane N-Fe-N directions and that the imidazole plane is nearly perpendicular to the g_X axis. Such an orientation is different from that reported in model compounds (12), where the in-plane EPR principal axes nearly bisect the two N-Fe-N directions of the porphyrin plane. This would be logical as the His orientation is one of the main factors that influence the g-tensor principal frame orientation.

In conclusion, our EPR and ENDOR data on *Anabaena* cytochrome c_6 point to the coexistence of two different conformations of the heme axial ligands for the oxidized state of the protein. In an isolated heme group, the orientation of the axial ligands should be the one more energetically favorable. Nevertheless, a change in the ligand orientation seems to require a small amount of energy (44). In the protein environment, the heme configuration is conditioned by the polypeptide chain structure. The ligand distances and orientations are responsible for the unpaired electron state and porphyrin ring shape (planar or distorted). In the case of redox proteins, these conditions have to be connected with the electron transfer mechanism to or from the heme center, so the protein can easily control the properties of its redox center. This would explain why heme proteins are a successful motif used by living organisms in many different biochemical processes. In cytochrome c_6 from *Anabaena* PCC 7119, the presence of two EPR forms (with putatively different heme axial ligand conformations) in the oxidized state should be related with reaction mechanisms. The coexistence of these two forms, possibly in a dynamical equilibrium, could be related to the fact that cytochrome c_6 is involved in two reactions: oxidation of cytochrome b_6f and reduction of the P700 reaction center of Photosystem I. Cytochrome c_6 may need some conformational flexibility to enable it to interact with different redox partners in these two independent processes. New efforts must be done in the characterization of this protein, from both the functional and the structural points of view, to further understand its electron transfer mechanism.

SUPPLEMENTARY MATERIAL

An online supplement to this article can be found by visiting BJ Online at http://www.biophysj.org.

This work was supported by Comisión Interministerial de Ciencia y Tecnología (CICYT, grants BQU2001-2520 and BIO2004-00279 to M.M., and BFU2005-07422-C02-02 to P.J.A.). It has been done within the GC program of Gobierno de Aragón (Grupos B18 and E33).

REFERENCES

1. Lowe, D. J. 1995. ENDOR and EPR of Metalloproteins. Springer, New York.
2. Hoffman, B. M. 2003. Electron-nuclear double resonance spectroscopy (and electron spin-echo envelope modulation spectroscopy) in bioinorganic chemistry. *Proc. Natl. Acad. Sci. USA.* 100:3575–3578.
3. Griffith, J. S. 1957. Theory of electron resonance in ferrihaemoglobin azide. *Nature.* 180:30–31.
4. Moore, G. R., and G. W. Pettigrew. 1990. Cytochromes *c*. Evolutionary, Structural and Physicochemical Aspects. Springer-Verlag, Berlin.
5. Brautigan, D. L., B. A. Feinberg, B. M. Hoffman, E. Margoliash, J. Peisach, and W. E. Blumberg. 1977. Multiple low spin forms of the cytochrome *c* ferrihemochrome. *J. Biol. Chem.* 252:574–582.
6. Gadsby, P. M. A., R. T. Hartshorn, J. J. G. Moura, J. D. Sinclair-Day, A. G. Sykes, and A. J. Thomson. 1989. Redox properties of the diheme cytochrome c_4 from *Azotobacter vinelandii* and characterisation of the two hemes by NMR, MCD, and EPR spectroscopy. *Biochim. Biophys. Acta.* 994:37–46.
7. Campos, A. P., A. P. Aguiar, M. Hervás, M. Regalla, J. A. Navarro, J. M. Ortega, A. V. Xavier, M. A. De la Rosa, and M. Teixeira. 1993. Cytochrome c_6 from *Monoraphidium braunii*. A cytochrome with an unusual heme axial coordination. *Eur. J. Biochem.* 216:329–341.
8. Teixeira, M., A. P. Campos, A. P. Aguiar, H. S. Costa, H. Santos, D. L. Turner, and A. V. Xavier. 1993. Pitfalls in assigning heme axial coordination by EPR. *c*-type cytochromes with atypical Met-His ligation. *FEBS Lett.* 317:233–236.
9. Arciero, D. M., Q. Peng, J. Peterson, and A. B. Hooper. 1994. Identification of axial ligands of cytochrome c_{552} from *Nitrosomonas europaea*. *FEBS Lett.* 342:217–220.
10. Inda, L. A., M. Medina, L. M. Saraiva, C. Gómez-Moreno, M. Teixeira, and M. L. Peleato. 1997. Characterisation of cytochrome c_6 from *Chlorella fusca*. *Photosynth. Res.* 54:107–114.
11. Scholes, C. P., and H. L. Van Camp. 1976. ENDOR from nitrogens and protons in low spin ferric heme and hemoproteins. *Biochim. Biophys. Acta.* 434:290–296.
12. Scholes, C. P., K. M. Falkowski, S. Chen, and J. Bank. 1986. Electron nuclear double resonance (ENDOR) of bis(imidazole)-ligated low-spin ferric heme systems. *J. Am. Chem. Soc.* 108:1660–1671.
13. Raitsimring, A. M., and F. A. Walker. 1998. Porphyrin and ligand protons as internal labels for determination of ligand orientation in ESEEMS of low-spin d^5 complexes in glassy media: ESEEM studies of the orientation of the **g** tensor with respect to the planes of axial ligands and porphyrin nitrogens of low-spin ferriheme systems. *J. Am. Chem. Soc.* 120:991–1002.
14. Fahnenschmidt, M., H. K. Rau, R. Bittl, W. Haehnel, and W. Lubitz. 1999. Characterization of a de novo designed heme protein by EPR and ENDOR spectroscopy. *Chem. Eur. J.* 5:2327–2334.
15. Fahnenschmidt, M., R. Bittl, H. K. Rau, W. Haehnel, and W. Lubitz. 2000. Electron paramagnetic resonance and electron nuclear double resonance spectroscopy of a heme protein maquette. *Chem. Phys. Lett.* 323:329–339.
16. Hoffman, B. M. 2003. ENDOR of metalloenzymes. *Acc. Chem. Res.* 36:522–529.
17. García-Rubio, I., J. I. Martínez, R. Picorel, I. Yruela, and P. J. Alonso. 2003. HYSCORE spectroscopy in the cytochrome b_{559} of the photosystem II reaction center. *J. Am. Chem. Soc.* 125:15846–15854.
18. Navarro, J. A., M. Hervás, and M. A. De la Rosa. 1997. Co-evolution of cytochrome c_6 and plastocyanin, mobile proteins transferring electrons from cytochrome b_6f to photosystem I. *J. Biol. Inorg. Chem.* 2:11–22.
19. Medina, M., R. O. Louro, J. Gagnon, M. L. Peleato, J. Mendes, C. Gómez-Moreno, A. V. Xavier, and M. Teixeira. 1997. Characterization

of cytochrome c_6 from cyanobacterium *Anabaena* PCC 7119. *J. Biol. Inorg. Chem.* 2:225–234.

20. Louro, R. O., M. Medina, A. P. Aguiar, M. Hervás, M. De la Rosa, C. Gómez-Moreno, D. L. Turner, and A. V. Xavier. 1998. Structural and magnetic characterisation of the haem core of ferricytochromes c_6. *J. Biol. Inorg. Chem.* 3:68–73.
21. Frazao, C., C. M. Soares, M. A. Carrondo, E. Pohl, Z. Dauter, K. S. Wilson, M. Hervás, J. A. Navarro, M. A. De la Rosa, and G. M. Sheldrick. 1995. *Ab initio* determination of the crystal structure of cytochrome c_6 and comparison with plastocyanin. *Structure.* 3:1159–1169.
22. Banci, L., I. Bertini, M. A. De la Rosa, D. Koulougliotis, J. A. Navarro, and O. Walter. 1998. Solution structure of oxidized cytochrome c_6 from the green alga *Monoraphidium braunii*. *Biochemistry.* 37:4831–4843.
23. Beissinger, M., H. Sticht, M. Sutter, A. Ejchart, W. Haehnel, and P. Rosch. 1998. Solution structure of cytochrome c_6 from the thermophilic cyanobacterium *Synechococcus elongatus*. *EMBO J.* 17:27–36.
24. Bes, M. T., E. Parisini, L. A. Inda, L. M. Saraiva, M. L. Peleato, and G. M. Sheldrick. 1999. Crystal structure determination at 1.4 Å resolution of ferredoxin from the green alga *Chlorella fusca*. *Structure.* 7:1201–1211.
25. Taylor, C. P. S. 1977. The EPR of low spin heme complexes. Relation of the t_{2g} hole model to the directional properties of the g tensor, and a new method for calculating the ligand field parameters. *Biochim. Biophys. Acta.* 491:137–149.
26. De Vries, S., and S. P. J. Albracht. 1979. Intensity of highly anisotropic low-spin heme EPR signals. *Biochim. Biophys. Acta.* 546:334–340.
27. Blumberg, W. E., and J. Peisach. 1971. A unified theory for low spin forms of all ferric heme proteins as studied by EPR. *In* Probes of Structure and Function of Macromolecules and Membranes. Vol. II. Probes of Enzymes and Hemoproteins. B. Chance, T. Yonetani, and A. S. Mildvan, editors. Academic Press, New York. 215–229.
28. Peisach, J., W. E. Blumberg, and A. Adler. 1973. Electron paramagnetic resonance studies of iron porphin and chlorin systems. *Ann. N. Y. Acad. Sci.* 206:310–327.
29. Astashkin, A. V., A. M. Raitsimring, and F. A. Walker. 2001. ^{1}H pulsed ENDOR and ESEEM evidence that the bis-imidazole complexes of iron(III) tetraphenylchlorin and tetraphenylporphyrin have the same order of g values, and the same electronic ground state. *J. Am. Chem. Soc.* 123:1905–1913.
30. Schweiger, A., and G. Jeschke. 2001. Principles of Pulse Electron Paramagnetic Resonance. Oxford University Press, Oxford.
31. Medina, M., A. Díaz, M. Hervás, J. A. Navarro, C. Gómez-Moreno, M. A. De la Rosa, and G. Tollin. 1993. A comparative laser- flash absorption spectroscopy study of *Anabaena* PCC7119 plastocyanin and cytochrome c_6 photooxidation by photosystem I particles. *Eur. J. Biochem.* 213:1133–1138.
32. Böhme, H., S. Brütsch, G. Weithmann, and P. Böger. 1980. Isolation and characterization of soluble cytochrome *c*-553 and membrane-bound cytochrome *f*-553 from thylakoids of the green alga *Scenedesmus acutus*. *Biochim. Biophys. Acta.* 590:248–260.
33. Stoll, S., and A. Schweiger. 2006. EasySpin, a comprehensive software package for spectral simulation and analysis in EPR. *J. Magn. Reson.* 178:42–55.
34. Walker, F. A. 1999. Magnetic spectroscopic (EPR, ESEEM, Mössbauer, MCD and NMR) studies of low-spin ferriheme centers and their corresponding heme proteins. *Coord. Chem. Rev.* 185–186: 471–534.
35. Hagen, W. R. 1989. *g*-Strain: inhomogeneous broadening in metalloprotein EPR. *In* Advanced EPR. Applications in Biology and Biochemistry. A. J. Hoff, editor. Elsevier, Amsterdam. 785–812.
36. Safo, M. K., G. P. Gupta, F. A. Walker, and W. R. Scheidt. 1991. Models of cytochromes *b*. Control of axial ligand orientation with a ''hindered'' porphyrin system. *J. Am. Chem. Soc.* 113:5497–5510.
37. Einsle, O., S. Foerster, K. Mann, G. Fritz, A. Messerschmidt, and P. M. H. Kroneck. 2001. Spectroscopic investigation and determination of reactivity and structure of the tetraheme cytochrome c_3 from *Desulfovibrio desulfuricans* Essex 6. *Eur. J. Biochem.* 268:3028–3035.
38. Aasa, R., and T. Vänngård. 1975. EPR signal intensity and powder shapes: a reexamination. *J. Magn. Reson.* 19:308–315.
39. Walker, F. A., D. Reis, and V. L. Balke. 1984. Models of the cytochromes *b*. 5. EPR studies of low-spin iron(III) tetraphenylporphyrins. *J. Am. Chem. Soc.* 106:6888–6898.
40. Shokhirev, N. V., and F. A. Walker. 1998. Co- and counterrotation of magnetic axes and axial ligands in low-spin ferriheme systems. *J. Am. Chem. Soc.* 120:981–990.
41. Walker, F. A., B. H. Huynh, W. R. Scheidt, and S. R. Osvath. 1986. Models of the cytochromes *b*. Effects of axial ligand plane orientation on the EPR and Mössbauer spectra of low-spin ferrihemes. *J. Am. Chem. Soc.* 108:5288–5297.
42. Quinn, R., J. S. Valentine, M. P. Byrn, and C. E. Strouse. 1987. Electronic structure of low-spin ferric porphyrins: a single-crystal EPR and structural investigation of the influence of axial ligand orientation and the effects of pseudo-Jahn-Teller distortion. *J. Am. Chem. Soc.* 109:3301–3308.
43. Turner, D. L. 1995. Determination of heme electronic structure in His-Met cytochromes *c* by C^{13} NMR-The effect of the axial ligands. *Eur. J. Biochem.* 227:829–837.
44. Medaković, V., and S. D. Zarić. 2003. Theoretical study on orientations of axially coordinated imidazoles in model systems of cytochromes. *Inorg. Chim. Acta.* 349:1–5.